Applied Catalysis B: Environmental 325 (2023) 122322

Contents lists available at ScienceDirect

Applied Catalysis B: Environmental

journal homepage: www.elsevier.com/locate/apcatb

High efficiency toluene electrooxidation at gas-solid interface on Nafion-modified SnO_2-Sb/Ti anode

Weiming Qian [a,b], Min Chen [a], Jianghao Zhang [a], Xueyan Chen [a], Jinhou Fang [c], Changbin Zhang [a,b,c,*]

[a] State Key Joint Laboratory of Environment Simulation and Pollution Control, Research Center for Eco-Environmental Sciences, Chinese Academy of Sciences, Beijing 100085, China
[b] University of Chinese Academy of Sciences, Beijing 100049, China
[c] Weifang Research Institute of Materials and Technology for Eco-Environmental Protection, Weifang, Shandong 261300, China

ARTICLE INFO

Keywords:
Electrochemical degradation
Gas-solid interface
Polymer modification

ABSTRACT

Electrocatalysis has been widely applied to treat organic compounds in wastewater; however, the efficient electrooxidation of gaseous organic compounds remains a significant challenge. Here, we fabricated a Nafion-modified SnO_2-Sb/Ti anode and assembled an all-solid reactor, achieving highly efficient electrooxidation of gaseous toluene. The anode coated with Nafion layer (Ti-SnO_2-Sb-10N) mineralized over 85 % toluene (35 ppm) with > 97 % CO_2 selectivity in 90 min at ambient temperature, in stark contrast to 8 % conversion over bare Ti-SnO_2-Sb under the same testing conditions. Based on the characterization results, we revealed that Nafion modification greatly increased the electrochemical active surface area (ECSA), accelerated the charge transfer, and also improved surface hydrophobicity. These three characteristics of Ti-SnO_2-Sb-10N significantly enhanced the production of hydroxyl radicals and optimized the reaction pathway, leading to high efficiency in gas-solid interface BTX electrooxidation.

1. Introduction

Volatile organic compounds (VOCs), such as benzene, toluene and xylene, are the major indoor air pollutants and are mainly released from indoor architectural decoration materials and combustion processes [1–4]. Indoor air VOCs show severe carcinogenic, mutagenic, and teratogenic effects on human health [5,6]. Since humans spend > 80 % of their lifetime indoors in modern society [7], there has been growing concern about indoor air pollution with rapid urbanization. Numerous efforts have been devoted to the abatement of indoor VOCs, and traditional techniques, including adsorption [8], catalytic combustion [9,10], plasma oxidation [11], and photocatalysis [12], etc., have been extensively investigated. However, these techniques still show limitations in practical application, such as insufficient adsorption capacity, high operation temperature, secondary pollution, safety risks, etc. Hence, developing an efficient technique suitable for indoor air purification is crucial.

Electrocatalysis is an environmentally friendly and promising technology due to its high efficiency and simple operation [13], which has been widely applied in wastewater treatments [14] but is rarely reported to remove gaseous pollutants. Govindan et al. tried to force gaseous trichloroethylene to dissolve in a solution and electro-scrub the targeted contaminant [15]. However, the electrochemical reaction efficiency of gaseous reactants with poor solubility in aqueous solutions is seriously limited by gas diffusion through the electrolyte to the catalyst surface [16]. Moreover, safety hazards caused by electrolyte solutions that are strongly acidic or alkaline have become essential restrictions on the application of electrochemical technology. Electrochemical oxidation at the gas-solid interface is a promising way to solve these problems. Recently, we employed a membrane electrode assembly (MEA) in an all-solid cell and established a gas-solid interface electrochemical oxidation system. By using antimony-doped tin dioxide coated on Ti foam (Ti-SnO_2-Sb) as an anode, we achieved the mineralization of benzene, toluene and xylene (BTX) at ambient temperature [17] and demonstrated the potential of this system for VOCs destruction under ambient conditions. However, the relatively poor current density in the gas-solid interface severely restricts the electrochemical reaction, and the system needs to be significantly improved for practical application.

* Corresponding author at: State Key Joint Laboratory of Environment Simulation and Pollution Control, Research Center for Eco-Environmental Sciences, Chinese Academy of Sciences, Beijing 100085, China.
E-mail address: cbzhang@rcees.ac.cn (C. Zhang).

https://doi.org/10.1016/j.apcatb.2022.122322
Received 28 September 2022; Received in revised form 6 December 2022; Accepted 21 December 2022
Available online 26 December 2022

Perfluorosulfonic acid ionomers (typically Nafion) are widely used in polymer electrolyte membrane fuel cells (PEMFCs) because of their chemical stability and outstanding proton conductivity [18]. Recently several studies have focused on how ionomers influence the activity and selectivity of various electrocatalytic reactions, such as carbon dioxide reduction (CO_2R) [19], Oxygen Reduction Reaction (ORR) [20], etc. In terms of the CO_2R reaction, the ionomer coating generally exhibits a positive effect on the performance of electrodes [21]. It has been revealed that coating a Nafion overlayer on a Cu electrode significantly increased the yield of CH_4 production by CO_2R because Nafion facilitated the stabilization of the Cu-CO* intermediate and allowed the stabilized CO to be protonated and further reduced to CH_4. However, the ionomers show adverse effects on the performance in several studied ORR cases. It was reported that a Nafion coating on Pt and Au electrodes occupied the active sites with its sulfonate groups, preventing oxygen molecules from reaching the active sites of the catalysts [22], significantly limiting the oxygen reduction reaction.

Self-supported electrodes such as Ti-SnO_2-Sb, where the active materials are grown in situ on the conductive substrates, generally do not need any modification but still work efficiently in wastewater treatment. However, we previously observed that Ti-SnO_2-Sb could not achieve a similar high efficiency for the mineralization of organic pollutants at the gas-solid interface as that demonstrated under solution conditions [27]. Considering the unique circumstance of the gas-solid interface and the potential of ionomers to promote the performance of the electrochemical reaction, we here fabricated a Nafion-coated Ti-Sb-SnO_2 anode pack, including a porous diffusion layer, catalyst and Nafion layer. The Sb-SnO_2 catalyst was deposited on the gas diffusion layer (foam Ti), and the Nafion was coated on the Sb-SnO_2 layer. The modified electrode was tested and carefully characterized by physicochemical and electrochemical methods. The Nafion-coated Ti-SnO_2-Sb anode could electrochemically oxidize over 85 % of toluene with 97 % CO_2 selectivity in 90 min at ambient temperature, while the bare Ti-SnO_2-Sb anode without modification could only convert 8 % of toluene. We reveal that Nafion coating increases the electrochemical active surface area (ECSA), modifies the surface hydrophobicity, and improves the proton transfer, leading to enhanced efficiency of toluene electrooxidation at the gas-solid interface.

2. Experimental

2.1. Preparation of electrodes

A piece of titanium foam (φ30 * 0.6 mm) was first put in acetone, ethanol and deionized water successively for ultrasonic washing treatment for 15 min to remove oil on its surface. A SnO_2-Sb layer was electrodeposited on the Ti foam at room temperature employing a two-electrode system (1 cm separation). The two-electrode system was composed of Ti foam as the cathode and Pt sheet as the anode in a solution containing 1 M $SnCl_2$ and 0.09 M $SbCl_3$. Dimethyl sulfoxide was used as the solvent for electrodeposition, promoting the formation of dense electrodeposited layers [23]. The Sn and Sb layer was obtained in the electrodeposition solution with a current density of 10 mA cm^{-2} for 0.5 h. The electrode was next heated in an oven at 773 K for two hours and then cooled in air. The Ti-SnO_2-Sb electrode was thus obtained. Next, 0.5 ml of Nafion solution (5 %, 10 %, 20 %, Dupont, USA) was dropped on the Ti-SnO_2-Sb electrode. After drying in an oven at 353 K for 30 min, the Ti-SnO_2-Sb-5N, Ti-SnO_2-Sb-10N, Ti-SnO_2-Sb-20N (Ti-SnO_2-Sb-mN, m is the concentration of Nafion solution) electrodes were obtained.

All cathodes were commercial gas diffusion electrodes. The cathode substrate was TGP-H-060 Toray carbon paper after hydrophobic treatment, with 1 mg/cm^2 Pt catalyst (Johnson Matthey 60 % Pt) loading.

2.2. Physicochemical characterization

The crystal structures of electrodes were investigated by X-ray diffraction (XRD, X pert Pro MPD X-ray powder diffractometer, Japan) using Cu Kα radiation over the range from 10° to 80° (2θ). To determine the surface elemental composition of the Nafion-coated and blank Ti-SnO_2-Sb electrodes, all samples were tested by X-ray photoelectron spectroscopy (XPS) using a scanning X-ray Microprobe (AXIS Ultra, Kratos Analytical, Inc.), and all peak positions were calibrated using the C1s peak at 284.8 eV. The surface morphologies of electrodes were studied by Field emission scanning electron microscopy (FE-SEM), using a SU-8020 electron microscope (Hitachi, Japan) coupled with an energy dispersive spectrometer (X-MAX, Oxford Instrument). The zeta potentials of electrodes were tested by a solid-surface Zeta potential instrument (Anton Paar, SurPASS 3, Austria). The water contact angles of the electrodes were tested with deionized water droplets by a Dataphysics OCA25 contact angle measurement system.

2.3. Electrochemical oxidation tests for toluene

The electrooxidation activity tests were conducted at room temperature. The self-designed all-solid reactor consists of two gas chambers separated by a proton membrane (Nafion N117, 175 μm thickness, 1100 EW) [24]. The reactant gas, which contained 35 ppm toluene, 20 % O_2 and N_2 balance, was circulated over the anode cell. The volume of reactant gas was 1.5 L, and the gas flow rate was 100 ml/min. The cathode cell was connected to the indoor atmosphere. The electrochemical reaction testing was conducted at different applied potentials at the gas-solid interface. All electrochemical tests were carried out in a conventional three-electrode system with a CHI760E electrochemical workstation (Chenhua Shanghai) on the self-designed reactor. The relative humidity was controlled by adjusting the gas flow rate through a water bubbler and monitored by a humidity sensor (HMP110, Vaisala). Toluene, CO_2, and CO concentrations were continuously measured using a GC-2014C gas chromatograph (Shimadzu, Japan) equipped with two flame ionization detectors (FID).

2.4. Electrochemical measurements

The electrochemical measurements were conducted in the self-designed two-cell reactor (shown in Figure S1) as described in our previous study [17] unless otherwise specified. Before the electrochemical oxidation tests for toluene, the Nafion 117 membrane was pretreated by a previously reported method to obtain a highly hydrated membrane[24]. Electrochemical measurements conducted in solutions were all carried out in 0.1 M Na_2SO_4 solution, in which Ag/AgCl (3 M KCl) served as the reference electrode and a Pt sheet (30 mm * 30 mm) as the counter electrode.

Cyclic voltammetry (CV) and linear sweep voltammetry (LSV) curves were measured with a scan rate of 10.0 mV s^{-1} at ambient conditions in the three-electrode system. ECSA was determined by the double-layer capacitance (C_{DL}) of the electrode by the following equation[25,26]:

$$ECSA = \frac{C_{DL}}{C_S} \quad (1)$$

The C_{DL} was measured with double-layer charging at various scan rates (the potential window was 0–0.8 V). C_s is the capacitance per unit area of an atomically smooth planar surface of the material under identical electrolyte conditions. A general value of $C_s = 0.060$ mF cm^{-2} is used in this work. Electrochemical impedance spectroscopy (EIS) was carried out with a potential amplitude of 5 mV. The frequency ranged from 1 Hz to 1 MHz.

2.5. ROS measurement

Electron paramagnetic resonance (EPR) spectra were measured at

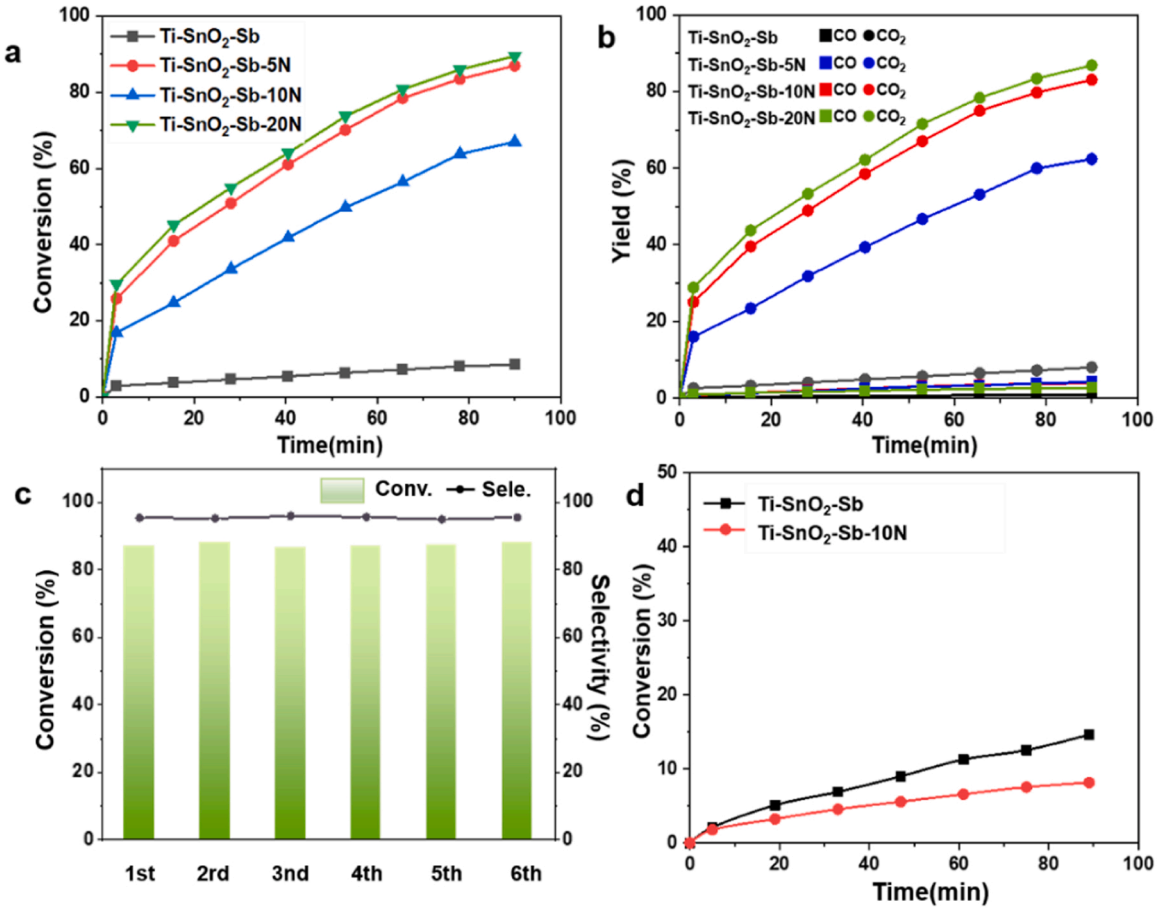

Fig. 1. Catalytic performance of catalysts in the electrochemical oxidation of toluene. Conversion (a) and yield of products (b) at 3 V. Reaction conditions: 35 ppm toluene, 20 vol% O_2, RH 100 % and N_2 balance; changes in toluene removal over six consecutive experiments (c); Catalytic performance of catalysts in the electrochemical oxidation of toluene without water vapor (35 ppm toluene, 20 vol% O_2, RH 0 % and N_2 balance) (d).

ambient temperature using a Bruker E500 EPR spectrometer to detect ·OH production during the reaction.

2.6. Energy consumption

The specific energy consumption (SEC, KWh/g) was calculated according to Eq. (2):

$$\mathrm{SEC} = \frac{UIt}{(TOC_{t0} - TOC_t)V} \tag{2}$$

where TOC_{t0} and TOC_t are the TOC at time t_0 and t, respectively, U is the applied voltage (V), I is the measured current (A), t is the electrolysis time (s), V is the volume of the treated gas (L).

The mineralization current efficiency was calculated by following Eq. (3):

$$\mathrm{MCE} = \frac{\Delta(TOC)_{\exp}}{\Delta(TOC)theor} \times 100\% \tag{3}$$

where $\Delta(\mathrm{TOC})_{\mathrm{theor}}$ is the theoretical value of removed TOC, which means all charge transfer is only consumed for mineralization reaction.

$$\Delta(TOC)_{theor} = \frac{\frac{It}{n_e F} \times n_c \times M}{V} \times 10^3 mg \cdot L^{-1} \tag{4}$$

where F is the Faraday constant (96,485 C mol^{-1}), n_e (n_e=35 for conversion to CO_2 or n_e = 21 for conversion to CO) is the number of electrons transfer and n_c (n_c = 7) is the carbon number of the organic compound. M (12 g mol^{-1}) is carbon atomic weight, I is the measured current (A), t is the electrolysis time (s), V is the volume of the treated gas (L).

3. Results

3.1. Activity tests for electrocatalytic oxidation of toluene

The as-prepared Ti-SnO_2-Sb, Ti-SnO_2-Sb-5N, Ti-SnO_2-Sb-10N and Ti-SnO_2-Sb-20N anodes were tested for the gas-solid interface electrocatalytic oxidation of toluene, and the results are shown in Fig. 1. Before the bias was applied, the reaction gas flows were maintained for an hour to reach toluene adsorption-desorption equilibrium in the reactor. When 3 V bias was applied, the Ti-SnO_2-Sb anode showed low activity for toluene oxidation with only 8 % conversion in 90 min. In contrast, the Nafion layer coating over Ti-SnO_2-Sb significantly improves the performance, and the conversions of toluene over Ti-SnO_2-Sb-5N and Ti-SnO_2-Sb-10N reach over 65 % and 85 % in 90 min (Fig. 1(a)). The Ti-SnO_2-Sb-20N anode shows similar performance to Ti-SnO_2-Sb-10N in the 90 min period, indicating that there exists an optimal Nafion layer coating content on Ti-SnO_2-Sb. Hence, we next mainly compare the behavior of Ti-SnO_2-Sb and Ti-SnO_2-Sb-10N to explore the promotion mechanism of Nafion modification.

The compositions of the gaseous products were analyzed by gas chromatography and a Fourier transform infrared spectrometer (FTIR) equipped with a gas cell. The test results show that the toluene completely converts to CO_2 and CO and no gaseous organic by-products are detected during the gas-solid interface electrocatalytic oxidation. Before and after the reaction, measurements of the elemental

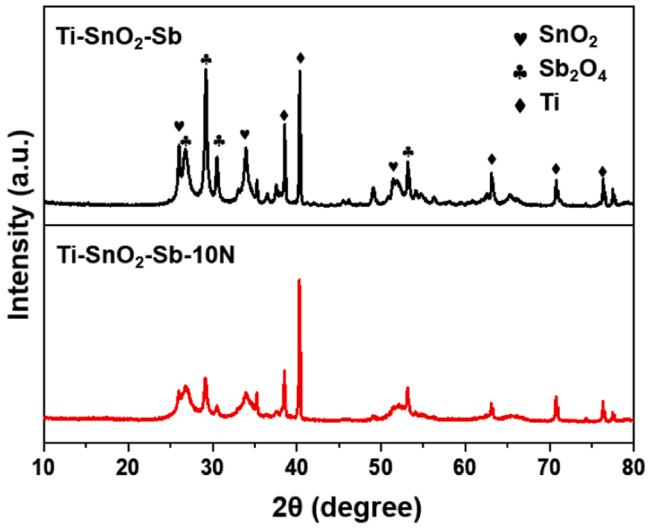

Fig. 2. XRD patterns of the Ti-SnO_2-Sb and Ti-SnO_2-Sb-10N electrodes.

composition of the electrodes (Table S2 and Table S3) do not show any apparent accumulation of intermediates on the surface. It can be concluded that no detectable gaseous or solid organic by-products appeared during the electrooxidation process. The yields of CO_2 and CO are calculated and displayed in Fig. 1(b). The coating of Nafion also promotes the conversion of toluene into CO_2. The CO_2 selectivities are 91 %, 94 % and 97 % over Ti-SnO_2-Sb, Ti-SnO_2-Sb-5N and Ti-SnO_2-Sb-10N after 90 min of reaction, respectively. We also calculated the specific energy consumption (SEC) and mineralization current efficiency (MCE). The SEC value for Ti-SnO_2-Sb and Ti-SnO_2-Sb-10N are 1.85 KWh/g and 0.60 KWh/g, and the MCE for Ti-SnO_2-Sb and Ti-SnO_2-Sb-10N electrodes are 1.82 % and 5.56 %, respectively, indicating that anode with the Nafion modification can consume less energy removing the same amount of organics. The MCE is relatively low compared with EO technology applied in wastewater treatments, which should be due to the low initial concentration of toluene. These results show that Nafion modification has a tremendously positive effect on the Ti-SnO_2-Sb in the gas-solid interface electrocatalytic oxidation of toluene, and the Nafion-modified Ti-SnO_2-Sb demonstrates a much higher performance than the unmodified one and also all the samples reported in our previous studies (Table S1).

The stability of the Ti-SnO_2-Sb-10N electrode was further investigated by repeated testing and the results are shown in Fig. 1(c). No apparent decrease in toluene conversion or CO_2 selectivity is observed over six cycles, indicating the high stability of Ti-SnO_2-Sb-10N. We also tested Ti-SnO_2-Sb and Ti-SnO_2-Sb-10N in the absence of water vapor (RH 0 %). As shown in Fig. 1(d), only 9 % and 15 % toluene conversion are achieved in 90 min on Ti-SnO_2-Sb-10N and Ti-SnO_2-Sb, respectively without detection of CO_x, indicating that toluene cannot be entirely oxidized without the presence of water vapor. These results, as well as our previous study, imply that the electrooxidation of toluene on the Ti-SnO_2-Sb electrode with/without a Nafion layer is mainly indirect oxidation [17,27].

3.2. Structural characterization

To further understand the promotion effect of a Nafion coating on the Ti-SnO_2-Sb electrode for the gas-solid interface electrooxidation of toluene, we next conducted structural characterization to obtain the physicochemical properties of the electrodes. Also, a series of electrochemical tests were carried out to explore the impact of Nafion in gas-solid interface electrocatalysis.

XRD patterns of the Ti-SnO_2-Sb and Ti-SnO_2-Sb-10N electrodes were first measured as shown in Fig. 2. The Ti-SnO_2-Sb sample exhibits the crystalline phases of the cassiterite SnO_2 (PDF# 41–1445) and Sb_2O_4 (PDF#71–0564), which is consistent with the reported results [28,29]. The diffraction peaks of the Ti substrate (PDF#65–3362) were evident on Ti-SnO_2-Sb, which can attribute to that the layer of active SnO_2-Sb is very thin and could be penetrated by X-rays. After being coated with Nafion, the peaks of SnO_2 and Sb_2O_4 become weak, indicating that the Nafion layer covers the Ti-SnO_2-Sb surface and blocks some of the X-rays. The peaks of metallic Ti remain in the Ti-SnO_2-Sb-10N spectra and the intensities only slightly decrease, suggesting that the Nafion molecules mainly cover the top surface of the electrode without entering the porous structure of the substrate.

The electronic states of elements in the Ti-SnO_2-Sb and Ti-SnO_2-Sb-10N electrodes were next analyzed by X-ray photoelectron spectroscopy (Figure S2). As shown in Fig. 3(a), there are no peaks in the scan range of Ti 2p (448–475 eV) [30] on both samples due to the covering of Ti by the SnO_2-Sb and Nafion layers. The XPS spectra of Ti-SnO_2-Sb exhibit peaks corresponding to Sn $3d_{5/2}$ (487.5 eV) and Sn $3d_{3/2}$ (496.4 eV), which can be assigned to the surface Sn^{4+} species [28]. Since the peaks of Sb $2p_{5/2}$ are overlapped with O 1 s peaks, the presence of Sb species is evidenced by the Sb $2p_{3/2}$ peak at about 541 eV [31]. The peak splitting results show that both Sb^{3+} and Sb^{5+} species exist on the Ti-SnO_2-Sb anode. After Nafion coating, the peaks related to Sn and Sb species disappear in the XPS spectrum of Ti-SnO_2-Sb-10N due to the covering by the Nafion layer. The S1s peak of -SO_3 groups at 170.2 eV, the C1s peak at around 293 eV, and the F1s peak at 689 eV ascribed to CF_2 are all detected, confirming the successful coating of the Nafion layer on the electrode surface [32].

Surface SEM images of Ti-SnO_2-Sb and Ti-SnO_2-Sb-10N samples are shown in Fig. 4 and Figure S3. The Ti-SnO_2-Sb sample shows a nanoflower structure. The thickness of the metal oxides (SnO_2-Sb layer) is about 35 μm as shown in Figure S4. Ti-SnO_2-Sb-10N shows the same morphology as the uncoated electrode, revealing a continuous and conformal ionomer layer, which corresponds to the Nafion layer [27,28,33]. The EDS analysis of Ti-SnO_2-Sb show Sn and Sb distribute homogeneously in the oxide films on the foam Ti. As shown in Fig. 4(b), F and C, the characteristic elements of Nafion, uniformly cover the surface of Ti-SnO_2-Sb. The elemental analysis results of Ti-SnO_2-Sb (Table S2) show that the Sn/Sb molar ratio is about 0.5, which is lower than that of the precursor solution (10:0.9), mainly due to Sb enrichment on the surface [34].

The Zeta potentials of Ti-SnO_2-Sb and Ti-SnO_2-Sb-10N were next tested in a neutral solution. The Zeta potential of Ti-SnO_2-Sb is 8 mV, while that of Ti-SnO_2-Sb-10N was − 6 mV. The $-SO_3^-$ groups in the Nafion layer are negatively charged and can attract the surface Sn^{4+} species and O-H groups[35]. Hence, an electrostatic interaction should exist between the positively charged SnO_2-Sb clusters and the negatively charged Nafion side chains [36]. The interaction between $-SO_3H$, -CF_2- in Nafion and −OH on SnO_2-Sb (−SO−H···HO−, −C−F−H···HO−) might also form hydrogen-bond networks between Nafion and SnO_2-Sb [37]. Hence, the Nafion could closely connect to surface SnO_2-Sb clusters due to electrostatic adsorption and hydrogen-bonding interactions.

Nafion consists of a poly-(tetra-fluoroethylene)- main backbone, which is hydrophobic, and pendant side chains with terminal sulfonic groups [18]. The hydrophilicity of the electrode was assumed to be changed by the Nafion layer coating. We measured the contact angles of water droplets on the surfaces of Ti-SnO_2-Sb and Ti-SnO_2-Sb-10N. Since the foam Ti substrates are permeable to water, we chose to test the contact angle of samples made with Ti plate without other changes. As shown in Fig. 4(a), the contact angle on Ti-SnO_2-Sb is 0°, indicating that the surface of Ti-SnO_2-Sb is entirely hydrophilic. As shown in Fig. 4(b), the Nafion coating layer improves the hydrophobicity of the Ti-SnO_2-Sb surface and the contact angle increases to 97°. Considering the competitive adsorption between H_2O and toluene on the electrode, the increased hydrophobicity of Ti-SnO_2-Sb-10N should be favorable for the adsorption and activation of toluene species.

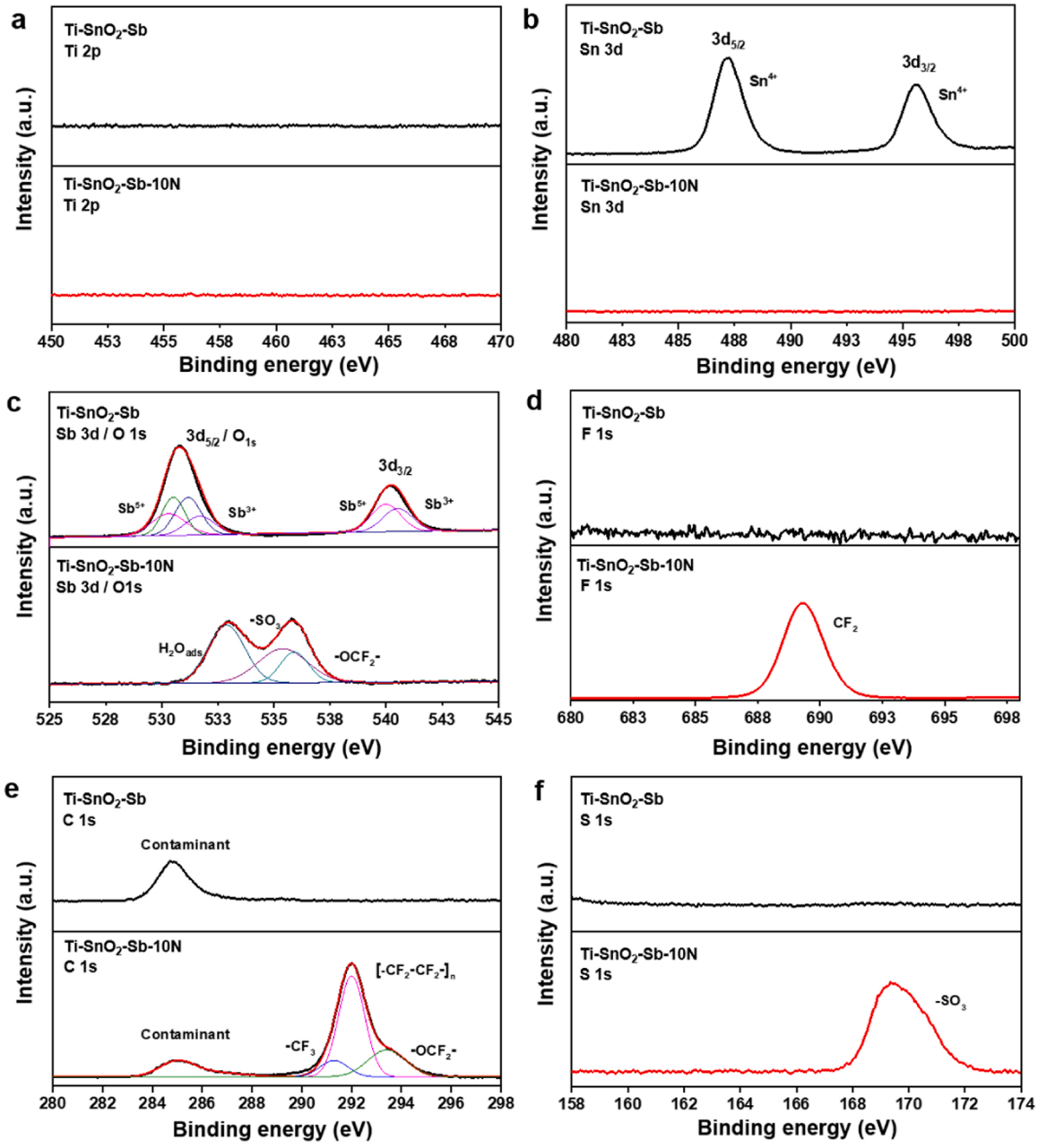

Fig. 3. XPS spectra of Sn 3d (a), O 1s (b), C 1s (c), S 1s (d), and F 1s (e) of Ti-SnO_2-Sb electrode (top row) and Ti-SnO_2-Sb-10N electrode (bottom row).

3.3. Electrochemical characterization

The electrochemical characterizations of Ti-SnO_2-Sb and Ti-SnO_2-Sb-10N were next explored in the gas-solid interface reactor mentioned above. Cyclic voltammetry (CV) experiments were carried out first. Fig. 5 shows the current flow changes as a function of cell voltage on Ti-SnO_2-Sb electrodes with and without a Nafion layer. Ti-SnO_2-Sb presents a current density of 1.6 mA cm^{-2} at a voltage of 3 V, while Ti-SnO_2-Sb-10N displays a current density of 10.3 mA cm^{-2} at 3 V, indicating that the Nafion coating layer significantly increases the current density, demonstrating the better electrocatalytic activity. We also carried out the CV measurements in the 0.1 M Na_2SO_4 solution and the results are presented in Figure S5. The CV curves of Ti-SnO_2-Sb and Ti-SnO_2-Sb-10N are similar, indicating that the Nafion modification has no influence on the activity of the SnO_2-Sb in the traditional solution conditions. These findings show that the Nafion overlayer could significantly promote the performance of Ti-SnO_2-Sb specifically in gas-solid interface electrooxidation.

LSV experiments were conducted under 35 ppm toluene to investigate whether direct oxidation could take place on the Ti-SnO_2-Sb and Ti-SnO_2-Sb-10N electrodes. As shown in Fig. 6(b), no pronounced oxidation peaks are observed in the Ti-SnO_2-Sb LSV curves. However, a pronounced oxidation peak appears at around 2.1 V in the LSV curves of Ti-SnO_2-Sb-10N, indicating that direct oxidation may occur in the electrooxidation of toluene. Direct oxidation over Ti-SnO_2-Sb-10N may contribute to the mineralization of toluene, which might be attributed to the increased hydrophobicity of the anode surface. As shown in Fig. 5, the Ti-SnO_2-Sb surface is completely hydrophilic, and the active sites would be covered by the surrounding hydration layer, hence toluene could not be readily adsorbed and activated. The Nafion coating increases the surface hydrophobicity of the Ti-SnO_2-Sb-10N, therefore some active sites could be available for toluene adsorption and activation at high humidity conditions, leading to direct oxidation. It has been reported that direct and indirect oxidation in conjunction could multiply

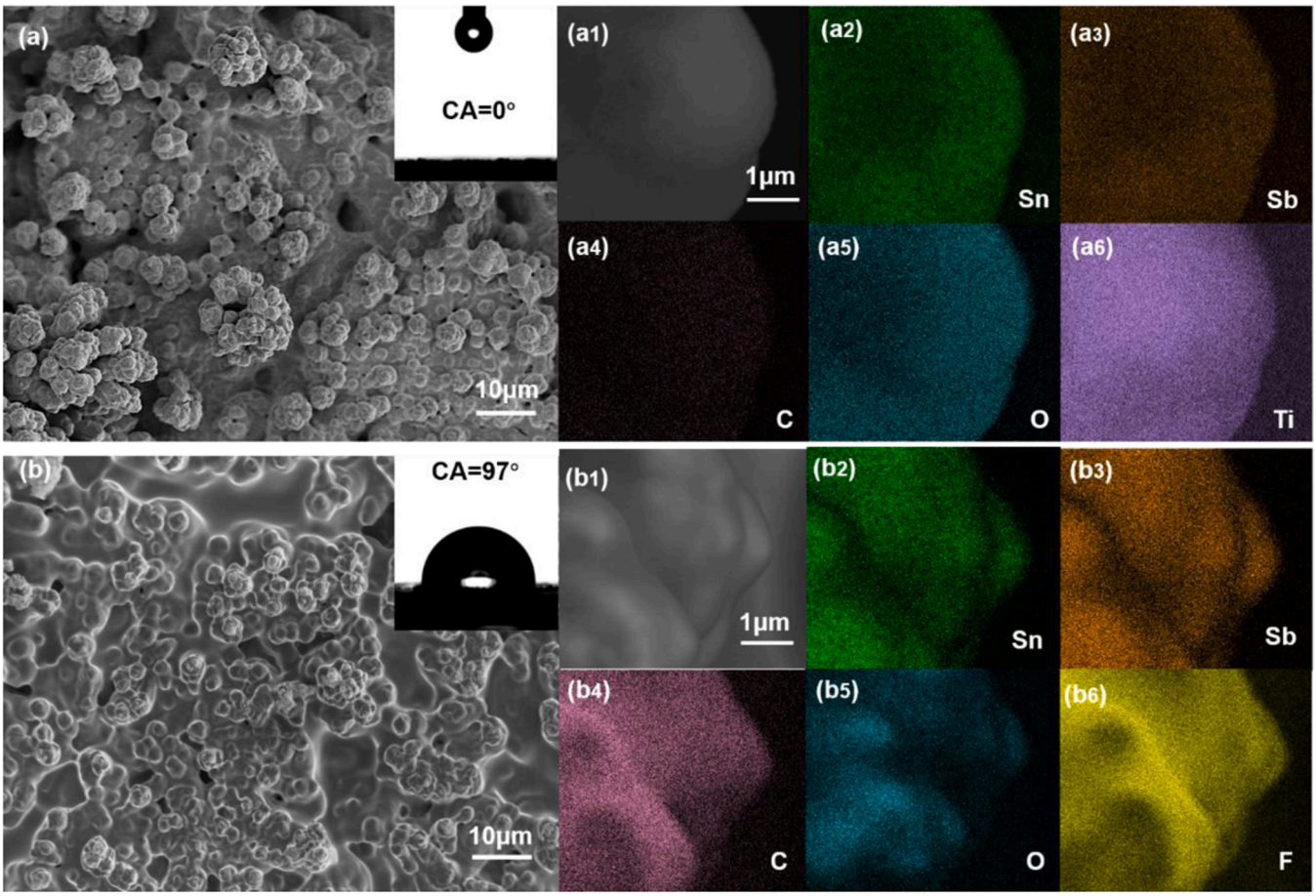

Fig. 4. Surface SEM images (a) of Ti-SnO_2-Sb and the corresponding elemental mapping (a1-a6) for Sn, Sb, C, O and Ti. SEM image of Ti-SnO_2-Sb-10N (b) and the corresponding elemental mapping images (b1-b6) for Sn, Sb, C, O and F. Insets in (a) and (b) are photographs of a droplet of deionized water on surfaces of Ti-SnO_2-Sb and Ti-SnO_2-Sb-10N.

the mineralization effect [38]. The unique differences in reaction mechanisms with and without the Nafion coating may be one of the critical reasons for the activity differences.

It is widely accepted that electrodes with larger ECSA can provide more active sites and have higher electrocatalytic activity [39]. The ECSA was measured via double-layer capacitance at the solid-gas interface. The ECSA of the two electrodes can be derived from the linear relation (Fig. 6a) of the current density (j) evolution with the scan rate (v) in the non-Faradaic regions (Fig. 6b and c), whose slopes can represent the electrical double-layer capacitance ($C_{dl} = \nu/j$). As shown in Fig. 6a, the ECSA of Ti-SnO_2-Sb-10N is much larger than that of Ti-SnO_2-Sb. Without the Nafion coating, the surfaces of Ti-SnO_2-Sb electrodes prepared by electrodeposition are relatively rough. As for the present gas-solid interface reactor, when we assembled the electrode pack by directly contacting the electrode with a solid electrolyte (Nafion membrane), the connection between the Ti-SnO_2-Sb and Nafion membrane was inadequate. After being coated with a Nafion layer, on the one hand, the layer could prevent the falling off of the catalyst from the foam Ti substrate; on the other hand, it could closely bond the surface Ti-SnO_2-Sb with the solid electrolyte (Nafion membrane), therefore helping more active sites participate in the reaction and greatly enhancing the ECSA of Ti-SnO_2-Sb-10N for the electrooxidation of toluene.

Next, electrochemical impedance spectroscopy (EIS) was used to further explore the effect of Nafion modification on charge transfer on Sb-SnO_2. The obtained Nyquist plots for each electrode in the self-designed reactor at different biases are shown in Fig. S6. Evident differences can be observed between Ti-SnO_2-Sb and Ti-SnO_2-Sb-10N from 1.2 V to 3 V in both the high and low-frequency regions. The EIS data were simulated by the equivalent circuit LR_Ω ($R_{ct}C_1$), where L, R_Ω and R_{ct} are the inductance, ohmic resistance and charge transfer resistance, and C_1 exhibits nonideal capacitance behavior because of surface porosity and heterogeneity [40]. R_{ct} values are very large below 1.5 V bias on both Ti-SnO_2-Sb and Ti-SnO_2-Sb-10N anodes, indicating that the charge transfer is very weak. With increasing the bias from 1.5 V to 3 V, R_{ct} gradually decreases. We compared the values of R_{ct} for each electrode and the results are shown in Table S4. The equivalent resistance (R_{ct}) of Ti-SnO_2-Sb-10N is much smaller than that of Ti-SnO_2-Sb at each bias, indicating that the Nafion layer dramatically promotes charge transfer after reaching an onset bias.

Fig. 7 shows the Nyquist plots with the representative bias of 3 V, and the fitted results are shown in Table 1. The ohmic resistance (R_Ω) consists of the electronic and ionic migration resistances and the contact resistance [41]. Considering that the ionic resistance within the electrolyte for the two anodes is the same, the difference in R_Ω could be due to electron conductivity and contact resistance. The Nafion layer is assumed to inhibit electron transfer, therefore the reduction in R_Ω confirms that the Nafion film decreases the contact resistance [42], which is partly counteracted by inhibiting electron transfer. The reduction in charge transfer resistance (R_{ct}) could be due to the excellent proton transfer capacity of the Nafion layer. A similar promotion effect has been also observed on the surface of Nafion-modified TiO_2 [43].

We believe that the hydrogen-bond networks formed between SnO_2-Sb and the Nafion chains play a vital role in transferring protons between the electrode and membrane. In the hydrogen-bond network, various sites, including Sn^{4+}, SO_4^{2-}, hydroxyls and water molecules adsorbed on the surface can all become proton carriers. Water molecules

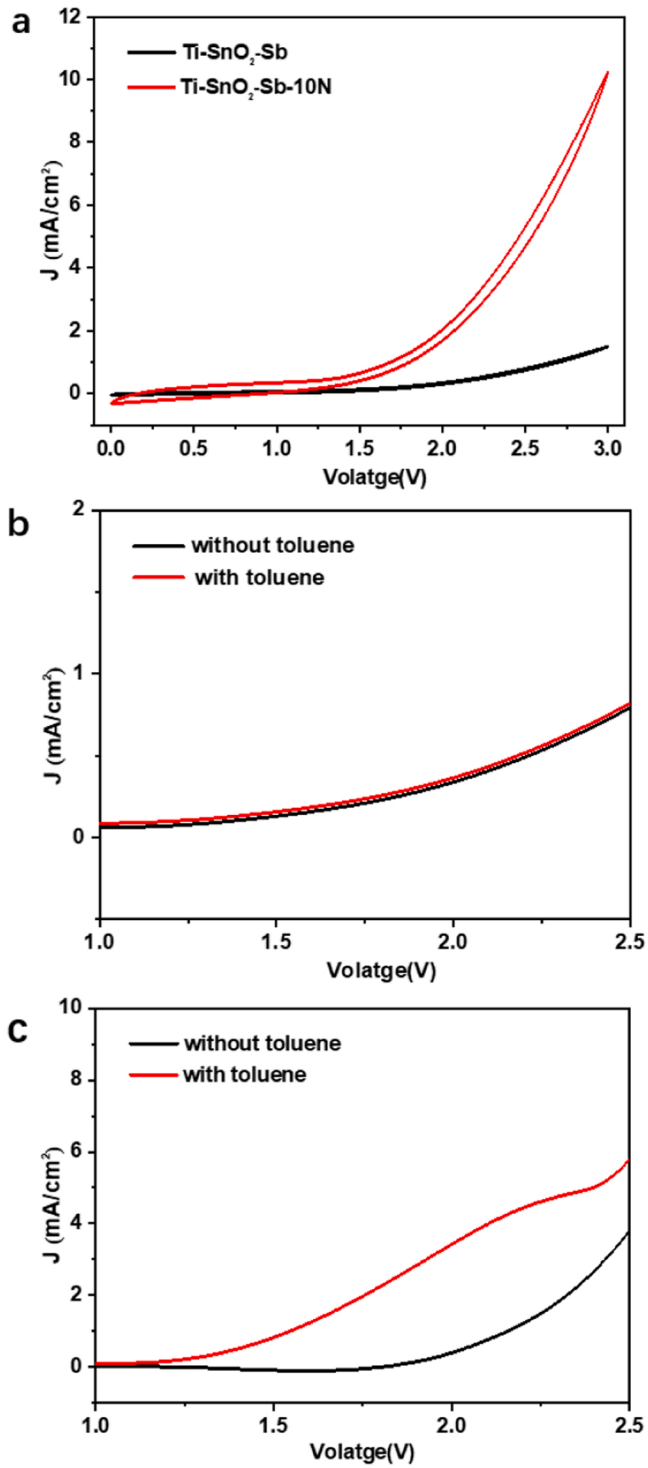

Fig. 5. CV curves of Ti-SnO_2-Sb and Ti-SnO_2-Sb-10N under N_2 gas at RH 100 % (a); LSV curves of Ti-SnO_2-Sb (b) and Ti-SnO_2-Sb-10N (c) with and without 35 ppm toluene at RH 100 %.

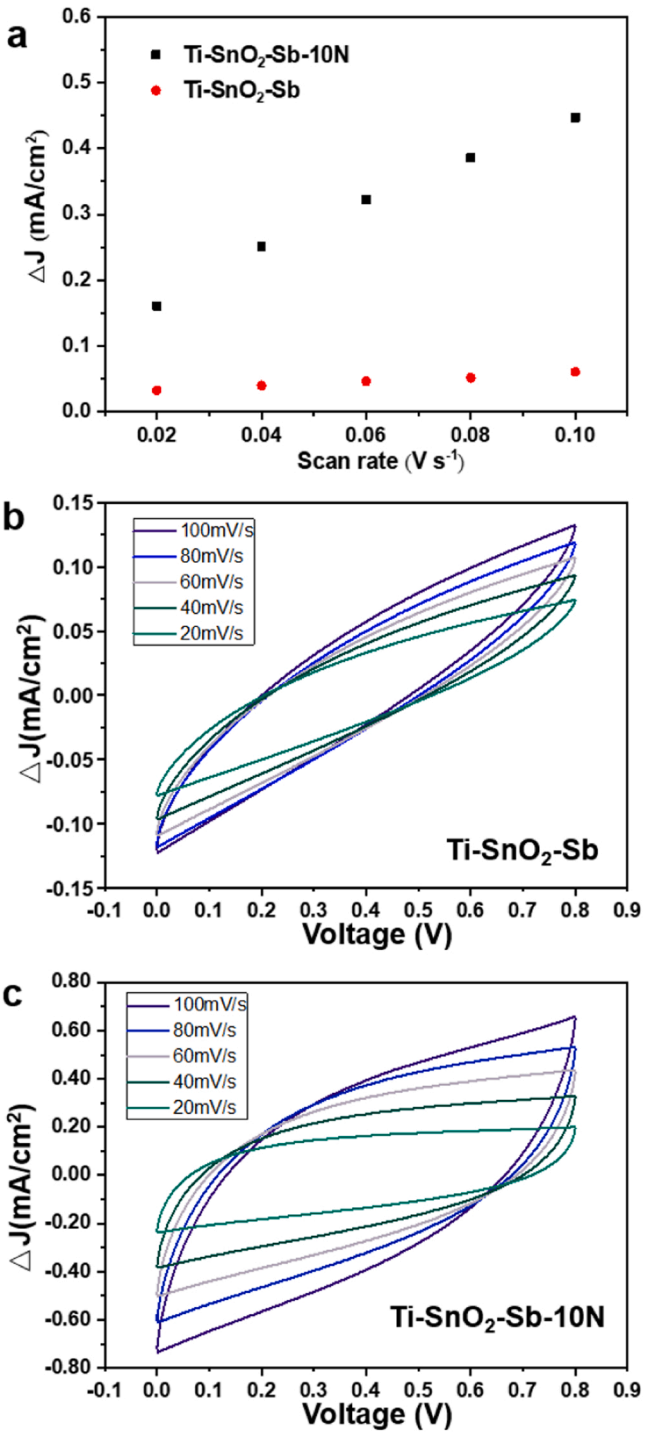

Fig. 6. (a) Charging current density difference plotted against scan rate at 0.4 V bias. CV curves of Ti-SnO_2-Sb-10N (b) and Ti-SnO_2-Sb (c) (bias window 0–0.8 V) at different scan rates.

in the hydrogen-bond networks are relatively mobile and have the same characteristics as those in the bulk liquid [44]. Hydrogen bonds can enable protons to migrate by rotating SO_4^{2-} and water molecules dynamically [45], which can be explained by the Grotthuss mechanism, greatly enhancing proton transport [46]. Without hydrogen-bond networks, protons transfer via proton carriers that diffuse freely, which can be explained by the vehicle mechanism, which would be slow [47]. Hence, the fast transfer of protons in the hydrogen-bond network induced by the Nafion coating should be the reason for the significantly reduced impedance of Ti-SnO_2-Sb-10N.

Our previous study showed that indirect oxidation via ·OH radicals was mainly responsible for the electrooxidation of toluene[17]. The reactions that take place in the electrode include water oxidation producing hydroxyl radical (·OH) and the reaction of ·OH with toluene. Toluene reacts with ·OH most forming phenolic intermediate (OH−toluene adducts) through hydrogen abstraction from the rings [48]. The OH−toluene adducts subsequently can react with O_2 at ambient conditions and finally convert to CO_x. Although oxygen and

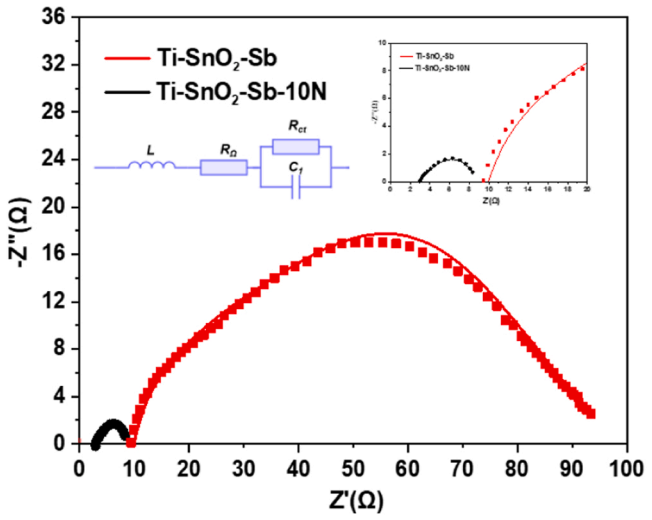

Fig. 7. Nyquist plots for Ti-SnO_2-Sb and Ti-SnO_2-Sb-10N (amplitude:5 mV, frequency ranges 1 Hz − 1 MHz).

Table 1
Fitted values of each circuit element/parameter for Ti-SnO_2-Sb and Ti-SnO_2-Sb-10N.[a]

Sample	L	R_Ω	R_{ct}	C_1	
	$E^{-6}H\ cm^2$	$\Omega\ cm^2$	$\Omega\ cm^2$	$C_{f,1}$ $F\ cm^{-2}\ s^{n-1}$	n_1
Ti-SnO_2-Sb	10.4	74.5	526.4	$2.03E^{-6}$	0.63
Ti-SnO_2-Sb-10N	6.1	11.3	44.15	$3.03E^{-4}$	0.56

[a] L, RΩ, Rct and C1 symbolize inductance, ohmic resistance, charge transfer resistance and EDL capacitance, respectively. Cf,1 is a frequency-independent constant related to ECSA, n1 is a factor ranging from 0 to 1 depending on the nature of the Cf.

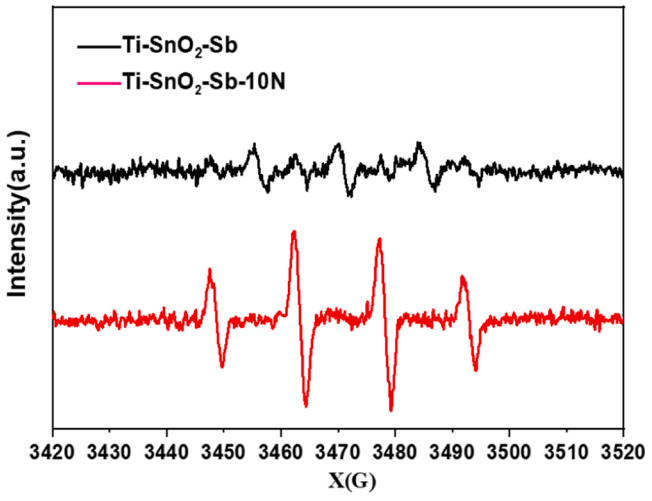

Fig. 8. DMPO spin-trapping EPR spectra measured at 303 K of Ti-SnO_2-Sb and Ti-SnO_2-Sb-10N.

·OH are both involved in the toluene mineralization, it is widely accepted that ·OH attack is the crux of the ring-opening reaction, which is the rate-determining step of toluene oxidation [49].

$$MO_x + H_2O \rightarrow MO_x(\cdot OH) + H^+ + e^- \ (M = \text{the anode surface}) \quad (5)$$

$$\text{Toluene} + \cdot OH \rightarrow CO_2 + H_2O \quad (6)$$

Previously, we detected the formation of ·OH on the surface of Ti-SnO_2-Sb at a bias of 2 V [17] by using a Laser-induced fluorescence (LIF) method, which is a reliable and efficient tool for directly detecting atmospheric ·OH [48]. Here, we employed electron paramagnetic resonance (EPR) spectroscopy to detect the formation of ·OH on Ti-SnO_2-Sb and Ti-SnO_2-Sb-10N, and the DMPO spin-trapping EPR spectra measured at 303 K are shown in Fig. 8. As we expected, the DMPO-·OH adducts signals of Ti-SnO_2-Sb are very weak. In contrast, Ti-SnO_2-Sb-10N presents four strong characteristic peaks of the DMPO-·OH adducts, indicating that many ·OH species are formed on Ti-SnO_2-Sb-10N. These results show that the Nafion coating significantly improves the production of ·OH on Ti-SnO_2-Sb-10N, which is direct evidence of the excellent electrochemical mineralization activity of Ti-SnO_2-Sb-10N.

4. Discussion

The Nafion layer over the SnO_2-Sb positively affects the ECSA, charge transport properties and hydrophobicity of the electrode. ECSA has a crucial impact on electrochemical activity because it determines the quantity of exposed active sites on which the reactants can absorb and react. When the Nafion solution is dropped on the Ti-SnO_2-Sb, it can permeate the entire electrode, and ionomer networks can be created spanning the SnO_2-Sb layer. The networks between the Nafion layer and SnO_2-Sb clusters can help more active sites closely contact the Nafion membranes, which, in turn, increases the ECSA significantly and is beneficial to the adsorption and activation of reactants. Moreover, the Nafion layer can prevent catalysts from falling off the foam Ti substrate, ensuring the stability of the electrodes.

The proton transfer from the SnO_2-Sb catalyst to the membrane plays a pivotal role in this reaction because the low transfer barrier allows H^+ to move rapidly toward the cathode and easily take part in the following reaction. EIS results measured at the gas-solid interface (Fig. 7) show that Nafion modification substantially decreased the charge transfer resistance. The hydrogen-bond networks between the Nafion and SnO_2-Sb might change the proton transfer mode from the vehicle mechanism to the Grotthuss mechanism. The optimization of the proton transfer pathway increases the mobility of protons and constructs a proton conduction channel. We have also conducted EIS measurements in Na_2SO_4 solution. The results show that the Nyquist plots of Ti-SnO_2-Sb and Ti-SnO_2-Sb-10N are analogous (Figure S7), indicating that they have similar charge transfer resistance under solution conditions. Hence, it could be concluded that proton transmission is a vital limiting factor at the gas-solid interface, differing from liquid-solid interface electrocatalysis.

The advantages of excellent ECSA and fast proton conduction on the Ti-SnO_2-Sb-10N electrode contribute to its high capacity for activating H_2O to produce ·OH species. The improved production of ·OH over Ti-SnO_2-Sb-10N is also related to the enhancement of the surface hydrophobicity by the Nafion layer coating. The generated ·OH can not only react with the target pollutant but also with water to produce oxygen ($MO_x(\bullet OH) + H_2O \rightarrow MO_x + O_2 + 2\ H^+$). When the electrode is more hydrophilic, the greater number of surface-adsorbed water molecules are favorable for reacting with ·OH radicals to produce oxygen, resulting in the loss of ·OH radicals [13]. When electrode surfaces become hydrophobic, hydroxyl radicals tend to be desorbed from the surfaces and free hydroxyl radicals are more likely to react with pollutants. Hence, the improvement in surface hydrophobicity increases the utilization efficiency of ·OH species. In addition, the enhanced hydrophobicity also promotes the adsorption and activation of toluene on the surface of the anode. The activated toluene could be directly oxidized to the intermediate products, which can be more easily mineralized by ·OH, further improving the reaction efficiency. All these factors, including larger ECSA, fast proton conduction, and enhanced surface hydrophobicity, contribute to the ·OH production and toluene mineralization.

Self-supported electrodes have been widely applied in many fields,

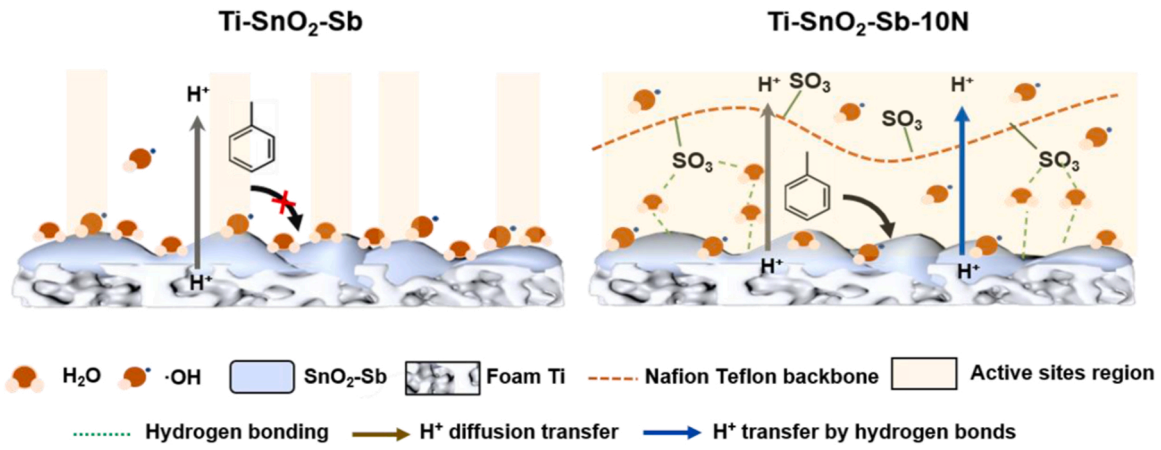

Scheme 1. Promotion mechanism of Nafion modification on Ti-SnO_2-Sb in gas-solid interface electrooxidation.

such as wastewater treatment, electrochemical water splitting, and so on [50]. Generally, under these solution conditions, self-supported electrodes work efficiently without the need for any modification since abundant catalytic sites are exposed to reactants with rapid charge transfer through the infiltration of the electrodes with the electrolyte. Nafion is the most widely used ionomer, serving as a dispersant for powder catalysts and also as a binder to avoid powder catalyst separation from substrates [52]. Our findings show that Nafion could optimize the self-supported electrodes when they are applied in solid electrolyte reactors by increasing ECSA, significantly promoting charge transfer and adjusting the hydrophobicity (as illustrated in Scheme 1). This promotion effect of Nafion coatings might be also applicable for other self-supported electrodes when they are employed in gas-solid interface electrocatalysis.

5. Conclusions

We prepared a Nafion-coated Ti-SnO_2-Sb catalyst, which demonstrated excellent performance in the gas-solid interface electrooxidation of toluene, achieving over 85 % conversion of toluene in 90 min with high selectivity of CO_2 (97 %). Modification by the Nafion layer enhances the connection between the electrode and solid electrolyte, significantly increasing the ESCA of the electrode. Moreover, Nafion modification promotes hydrogen-bond network formation, which accelerates the proton transport on the Ti-SnO_2-Sb-10N surface. The Nafion layer also improves the hydrophobicity of the electrode surface, which facilitates toluene adsorption and subsequent direct oxidation on the anode, and is also beneficial to the enrichment of free ·OH radicals. These three characteristics of Ti-SnO_2-Sb-10N together account for the significant increase in the mineralization activity of Ti-SnO_2-Sb-10N in toluene oxidation. Our study demonstrates how Nafion modification impacts Ti-SnO_2-Sb electrodes in the gas-solid interface electrooxidation reaction. Our findings provide an efficient strategy for the future design of high-performance self-supported electrodes employed for gas-solid interface electrocatalysis.

CRediT authorship contribution statement

Weiming Qian: Methodology, Data curation, Formal analysis, Investigation, Data curation, Visualization, Writing – original draft. **Min Chen:** Resources, Data curation, Characterization. **Jianghao Zhang:** Formal analysis, Writing – review & editing. **Xueyan Chen:** Methodology, Validation. **Changbin Zhang:** Writing – original draft, Writing – review & editing, Supervision, Project administration, Funding acquisition.

Declaration of Competing Interest

The authors declare that they have no known competing financial interests or personal relationships that could have appeared to influence the work reported in this paper.

Data Availability

Data will be made available on request.

Acknowledgments

This work was financially supported by the National Natural Science Foundation of China (22025604, 21976196, 21936005) and by the National Key R&D Program of China (2022YFC3800404).

Appendix A. Supporting information

Supplementary data associated with this article can be found in the online version at doi:10.1016/j.apcatb.2022.122322.

References

[1] G. de Gennaro, G. Farella, A. Marzocca, A. Mazzone, M. Tutino, Indoor and outdoor monitoring of volatile organic compounds in school buildings: indicators based on health risk assessment to single out critical issues, Int. J. Environ. Res. Public Health 10 (2013) 6273–6291, https://doi.org/10.3390/ijerph10126273.
[2] A.T. Hodgson, D. Beal, J.E.R. McIlvaine, Sources of formaldehyde, other aldehydes and terpenes in a new manufactured house, Indoor Air 12 (2002) 235–242, https://doi.org/10.1034/j.1600-0668.2002.01129.x.
[3] D.A. Sarigiannis, S.P. Karakitsios, A. Gotti, I.L. Liakos, A. Katsoyiannis, Exposure to major volatile organic compounds and carbonyls in European indoor environments and associated health risk, Environ. Int. 37 (2011) 743–765, https://doi.org/10.1016/j.envint.2011.01.005.
[4] C. Billionnet, E. Gay, S. Kirchner, B. Leynaert, I. Annesi-Maesano, Quantitative assessments of indoor air pollution and respiratory health in a population-based sample of French dwellings, Environ. Res. 111 (2011) 425–434, https://doi.org/10.1016/j.envres.2011.02.008.
[5] A.P. Jones, Chapter 3 Indoor air quality and health, Dev. Environ. Sci. 1 (2002) 57–115, https://doi.org/10.1016/S1474-8177(02)80006-7.
[6] C. Rösch, T. Kohajda, S. Röder, M. von Bergen, U. Schlink, Relationship between sources and patterns of VOCs in indoor air, Atmos. Pollut. Res. 5 (2014) 129–137, https://doi.org/10.5094/APR.2014.016.
[7] M. Cetin, H. Sevik, Measuring the impact of selected plants on indoor CO_2 concentrations, Pol. J. Environ. Stud. 25 (2016) 973–979, https://doi.org/10.15244/pjoes/61744.
[8] C.J.G. Jou, H.S. Tai, Application of granulated activated carbon packed-bed reactor in microwave radiation field to treat BTX, Chemosphere 37 (1998) 685–698, https://doi.org/10.1016/S0045-6535(98)00084-8.
[9] M. Piumetti, D. Fino, N. Russo, Mesoporous manganese oxides prepared by solution combustion synthesis as catalysts for the total oxidation of VOCs, Appl. Catal. B Environ. 163 (2015) 277–287, https://doi.org/10.1016/j.apcatb.2014.08.012.
[10] X. Qian, D. Yue, Z. Tian, M. Reng, Y. Zhu, M. Kan, T. Zhang, Carbon quantum dots decorated Bi 2 WO 6 nanocomposite with enhanced photocatalytic oxidation

activity for VOCs, Appl. Catal. B Environ. 193 (2016) 16–21, https://doi.org/10.1016/j.apcatb.2016.04.009.
[11] H.H. Kim, A. Ogata, S. Futamura, Oxygen partial pressure-dependent behavior of various catalysts for the total oxidation of VOCs using cycled system of adsorption and oxygen plasma, Appl. Catal. B Environ. 79 (2008) 356–367, https://doi.org/10.1016/j.apcatb.2007.10.038.
[12] W.K. Jo, K.H. Park, Heterogeneous photocatalysis of aromatic and chlorinated volatile organic compounds (VOCs) for non-occupational indoor air application, Chemosphere 57 (2004) 555–565, https://doi.org/10.1016/j.chemosphere.2004.08.018.
[13] J. Radjenovic, D.L. Sedlak, Challenges and opportunities for electrochemical processes as next-generation technologies for the treatment of contaminated water, Environ. Sci. Technol. 49 (2015) 11292–11302, https://doi.org/10.1021/acs.est.5b02414.
[14] H. Kim, J. Lim, S. Lee, H.H. Kim, C. Lee, J. Lee, W. Choi, Spontaneous generation of H_2O_2 and hydroxyl radical through O_2 reduction on copper phosphide under ambient aqueous condition, Environ. Sci. Technol. 53 (2019) 2918–2925, https://doi.org/10.1021/acs.est.8b06353.
[15] M. Govindan, R.A. Gopal, I.S. Moon, Efficient removal of gaseous trichloroethylene by continuous feed electro-scrubbing using a new homogeneous heterobimetallic, Chem. Eng. J. 308 (2017) 1145–1153, https://doi.org/10.1016/j.cej.2016.09.137.
[16] Q. Zhang, M. Zhou, X. Du, Highly efficient electrosynthesis of hydrogen peroxide on a superhydrophobic three-phase interface by natural air diffusion, Nat. Commun. 11 (2020) 1–11, https://doi.org/10.1038/s41467-020-15597-y.
[17] B. Zhang, M. Chen, L. Wang, X. Zhao, R. Hu, H. Chen, P. Xie, C. Zhang, H. He, Electrochemical oxidation of volatile organic compounds in all-solid cell at ambient temperature, Chem. Eng. J. 354 (2018) 93–104, https://doi.org/10.1016/j.cej.2018.07.208.
[18] H. Zhang, P.K. Shen, Recent development of polymer electrolyte membranes for fuel cells, Chem. Rev. 112 (2012) 2780–2832, https://doi.org/10.1021/cr200035s.
[19] D.M. Koshy, S.A. Akhade, A. Shugar, K. Abiose, J. Shi, S. Liang, J.S. Oakdale, S. E. Weitzner, J.B. Varley, E.B. Duoss, S.E. Baker, C. Hahn, Z. Bao, T.F. Jaramillo, Chemical modifications of Ag catalyst surfaces with imidazolium ionomers modulate H_2 evolution rates during electrochemical CO_2 Reduction, J. Am. Chem. Soc. 143 (2021) 14712–14725, https://doi.org/10.1021/jacs.1c06212.
[20] J. Tymoczko, F. Calle-Vallejo, V. Colic, M.T.M. Koper, W. Schuhmann, A. S. Bandarenka, Oxygen reduction at a Cu-modified Pt(111) model electrocatalyst in contact with nafion polymer, ACS Catal. 4 (2014) 3772–3778, https://doi.org/10.1021/cs501037y.
[21] H. Pan, C.J. Barile, Electrochemical CO_2 reduction to methane with remarkably high Faradaic efficiency in the presence of a proton permeable membrane, Energy Environ. Sci. 13 (2020) 3567–3578, https://doi.org/10.1039/d0ee02189j.
[22] J. Zeng, D.I. Jean, C. Ji, S. Zou, In situ surface-enhanced raman spectroscopic studies of Nafion adsorption on Au and Pt electrodes, Langmuir 28 (2012) 957–964, https://doi.org/10.1021/la2035455.
[23] Y. Duan, Y. Chen, Q. Wen, T. Duan, Electrodeposition preparation of a cauliflower-like Sb-SnO_2 electrode from DMSO solution for electrochemical dye decolorization, RSC Adv. 6 (2016) 48043–48048, https://doi.org/10.1039/c6ra07744g.
[24] I.C. Gonçalves, W.T.P. Dos Santos, D.V. Franco, L.M. Da Silva, Fabrication and characterization of oxide fine-mesh electrodes composed of Sb-SnO_2 and study of oxygen evolution from the electrolysis of electrolyte-free water in a solid polymer electrolyte filter-press cell: Possibilities for the combustion of organic, Electrochim. Acta 121 (2014) 1–14, https://doi.org/10.1016/j.electacta.2013.12.119.
[25] X. Wei, X. Wen, Y. Liu, C. Chen, C. Xie, D. Wang, M. Qiu, N. He, P. Zhou, W. Chen, J. Cheng, H. Lin, J. Jia, X.-Z. Fu, S. Wang, Oxygen vacancy-mediated selective C–N coupling toward electrocatalytic urea synthesis, J. Am. Chem. Soc. 144 (2022) 11530–11535, https://doi.org/10.1021/jacs.2c03452.
[26] Y. Qi, Y. Zhang, L. Yang, Y. Zhao, Y. Zhu, H. Jiang, C. Li, Insights into the activity of nickel boride/nickel heterostructures for efficient methanol electrooxidation, Nat. Commun. 13 (1) (2022) 1–11, https://doi.org/10.1038/s41467-022-32443-5.
[27] N. Oturan, J. Wu, H. Zhang, V.K. Sharma, M.A. Oturan, Electrocatalytic destruction of the antibiotic tetracycline in aqueous medium by electrochemical advanced oxidation processes: effect of electrode materials, Appl. Catal. B Environ. 141 (2013) 92–97, https://doi.org/10.1016/j.apcatb.2013.03.035.
[28] C. Yang, Y. Fan, P. Li, Q. Gu, X. Yan Li, Freestanding 3-dimensional macro-porous SnO_2 electrodes for efficient electrochemical degradation of antibiotics in wastewater, Chem. Eng. J. 422 (2021), https://doi.org/10.1016/j.cej.2021.130032.
[29] A. Ansari, D. Nematollahi, Environmental Convergent paired electrocatalytic degradation of p-dinitrobenzene by Ti/SnO_2-Sb/β-PbO_2 anode. A new insight into the electrochemical degradation mechanism, Appl. Catal. B Environ. 261 (2020), 118226, https://doi.org/10.1016/j.apcatb.2019.118226.
[30] G. Zhao, Y. Zhang, Y. Lei, L.V. Baoying, J. Gao, Y. Zhang, D. Li, Fabrication and electrochemical treatment application of a novel lead dioxide anode with superhydrophobic surfaces, high oxygen evolution potential, and oxidation capability, Environ. Sci. Technol. 44 (2010) 1754–1759, https://doi.org/10.1021/es902336d.
[31] S. Man, H. Bao, K. Xu, H. Yang, Q. Sun, L. Xu, W. Yang, Z. Mo, X. Li, Preparation and characterization of Nd-Sb co-doped SnO_2 nanoflower electrode by hydrothermal method for the degradation of norfloxacin, Chem. Eng. J. 417 (2021), 129266, https://doi.org/10.1016/j.cej.2021.129266.
[32] M. Wang, L. Wan, J. Luo, Promoting CO_2 electroreduction on CuO nanowires with a hydrophobic Nafion overlayer, Nanoscale 13 (2021) 3588–3593, https://doi.org/10.1039/d0nr08369k.
[33] F.P. García de Arquer, C.T. Dinh, A. Ozden, J. Wicks, C. McCallum, A.R. Kirmani, D.H. Nam, C. Gabardo, A. Seifitokaldani, X. Wang, Y.C. Li, F. Li, J. Edwards, L. J. Richter, S.J. Thorpe, D. Sinton, E.H. Sargent, CO_2 electrolysis to multicarbon products at activities greater than 1 A cm-2, Science 367 (2020) (2020) 661–666, https://doi.org/10.1126/science.aay4217.
[34] A. De Battisti, S. Barison, S. Daolio, J.L. Va, U.V. De Alicante, A. De Correos, Preparation and characterization of antimony-doped tin dioxide electrodes, 3. XPS SIMS Charact. (2004) 15976–15981.
[35] P. Zhang, Y. Chen, S. Wu, X. Li, M. Liu, S. Li, Enhancing the performance of n-i-p perovskite solar cells by introducing hydroxyethylpiperazine ethane sulfonic acid for interfacial adjustment, Nanoscale 14 (2022) 35–41, https://doi.org/10.1039/d1nr05939d.
[36] B. Liu, B. Hu, J. Du, D. Cheng, H.Y. Zang, X. Ge, H. Tan, Y. Wang, X. Duan, Z. Jin, W. Zhang, Y. Li, Z. Su, Precise molecular-level modification of nafion with bismuth oxide clusters for high-performance proton-exchange membranes, Angew. Chem. Int. Ed. 60 (2021) 6076–6085, https://doi.org/10.1002/anie.202012079.
[37] W. Chen, M. Chen, D. Zhen, T. Li, X. Wu, S. Tang, L. Wan, S. Zhang, G. He, SO_4^{2-}/SnO_2 solid superacid granular stacked one-dimensional hollow nanofiber for a highly conductive proton-exchange membrane, ACS Appl. Mater. Interfaces 12 (2020) 40740–40748, https://doi.org/10.1021/acsami.0c09122.
[38] K. Wang, K. Zhao, X. Qin, S. Chen, H. Yu, X. Quan, Treatment of organic wastewater by a synergic electrocatalysis process with Ti^{3+} self-doped TiO_2 nanotube arrays electrode as both cathode and anode, J. Hazard. Mater. 424 (2022), 127747, https://doi.org/10.1016/j.jhazmat.2021.127747.
[39] J.X. Feng, S.Y. Tong, Y.X. Tong, G.R. Li, Pt-like hydrogen evolution electrocatalysis on PANI/CoP hybrid nanowires by weakening the shackles of hydrogen ions on the surfaces of catalysts, J. Am. Chem. Soc. 140 (2018) 5118–5126, https://doi.org/10.1021/jacs.7b12968.
[40] G.F. Li, D. Yang, P.Y.Abel Chuang, Defining nafion ionomer roles for enhancing alkaline oxygen evolution electrocatalysis, ACS Catal. 8 (2018) 11688–11698, https://doi.org/10.1021/acscatal.8b02217.
[41] K.R. Cooper, M. Smith, Electrical test methods for on-line fuel cell ohmic resistance measurement, J. Power Sources 160 (2006) 1088–1095, https://doi.org/10.1016/j.jpowsour.2006.02.086.
[42] C.M. Lai, J.C. Lin, F.P. Ting, S. Der Chyou, K.L. Hsueh, Contribution of Nafion loading to the activity of catalysts and the performance of PEMFC, Int. J. Hydrogen Energy 33 (2008) 4132–4137, https://doi.org/10.1016/j.ijhydene.2008.05.074.
[43] W. Kim, T. Seok, W. Choi, Nafion layer-enhanced photosynthetic conversion of CO_2 into hydrocarbons on TiO_2 nanoparticles, Energy Environ. Sci. 5 (2012) 6066–6070, https://doi.org/10.1039/c2ee03338k.
[44] Y. Zhen, J. Zhang, W. Wang, Y. Li, X. Gao, H. Xue, X. Liu, Z. Jia, Q. Xue, J. Zhang, Y. Yan, N.S. Alharbi, T. Hayat, Embedded SnO_2/Diatomaceous earth composites for fast humidity sensing and controlling properties, Sens. Actuators B Chem. 303 (2020), 127137, https://doi.org/10.1016/j.snb.2019.127137.
[45] V. Ponomareva, G. Lavrova, Controlling the proton transport properties of solid acids via structural and microstructural modification, J. Solid State Electrochem. 15 (2011) 213–221, https://doi.org/10.1007/s10008-010-1227-1.
[46] V.K. Tomer, S. Duhan, A facile nanocasting synthesis of mesoporous Ag-doped SnO_2 nanostructures with enhanced humidity sensing performance, Sens. Actuators B Chem. 223 (2016) 750–760, https://doi.org/10.1016/j.snb.2015.09.139.
[47] S.Y. Lee, A. Ogawa, M. Kanno, H. Nakamoto, T. Yasuda, M. Watanabe, Nonhumidified intermediate temperature fuel cells using protic ionic liquids, J. Am. Chem. Soc. 132 (2010) 9764–9773, https://doi.org/10.1021/ja102367x.
[48] S. Gligorovski, R. Strekowski, S. Barbati, D. Vione, Environmental implications of hydroxyl radicals (·OH), Chem. Rev. 115 (2015) 13051–13092, https://doi.org/10.1021/cr500310b.
[49] I. Suh, R. Zhang, L.T. Molina, M.J. Molina, Oxidation mechanism of aromatic peroxy and bicyclic radicals from OH-toluene reactions, J. Am. Chem. Soc. 125 (2003) 12655–12665, https://doi.org/10.1021/ja0350280.
[50] H. Sun, Z. Yan, F. Liu, W. Xu, F. Cheng, J. Chen, Self-supported transition-metal-based electrocatalysts for hydrogen and oxygen evolution, Adv. Mater. 32 (2020) 1806326, https://doi.org/10.1002/adma.201806326.